

Correlated second-order Dirac semimetals with Coulomb interactions

Yu-Wen Lee*

Department of Applied Physics, Tunghai University, Taichung, Taiwan, R.O.C.

Yu-Li Lee†

Department of Physics, National Changhua University of Education, Changhua, Taiwan, R.O.C.

(Dated: September 7, 2021)

We investigate the effects of long range Coulomb interactions on the low-temperature properties of a second-order Dirac semimetal in terms of the renormalization group. In contrast to the first-order Dirac semimetal, the full rotation symmetry is broken even in the continuum limit, and thus the low-energy physics is controlled by two dimensionless parameters: the dimensionless coupling constant and the ratio of the anisotropy parameters. We show that the former flows to zero and the latter flows to a fixed value at low energies. Thus, one may calculate physical quantities in terms of the renormalized perturbation theory. As an application, we determine the temperature dependence of the specific heat by solving the renormalization-group equations. Following from the breaking of the full rotation symmetry, there exists a crossover temperature scale T_c (and a length scale L_c). Physical quantities approach the values for the first-order Dirac semimetal only when the temperature is much smaller than T_c . Similarly, the screened Coulomb potential will become anisotropic when the distance is smaller than L_c , while the unscreened form is recovered at its tail.

I. INTRODUCTION

In the past 15 years, topological phases of matters have become an active research topic in condensed matter physics. Among these phases, there are gapped systems, such as topological insulators (TIs) and topological superconductors (TSCs)¹⁻³, and gapless systems such as Weyl semimetals (WSMs)^{4,5} and various variants, e.g., anisotropic Weyl fermions⁶, double WSMs^{7,8}, and tilted WSMs⁹. For the TIs, the bulk topology are usually indicated by some topological indices, and it is characterized by the monopole charges in the momentum space for the WSMs. In these systems, the bulk topology is protected by some (global) symmetries³, and thus are dubbed as the symmetry protected topological (SPT) phases. For these samples with boundaries, there are gapless states localized at the edges, known as the bulk-boundary correspondence. These gapless edge states is stable against symmetry-preserving perturbations.

Later, the study of topological phases was extended to higher order and the previous mentioned TIs now belong to the class of the first order¹⁰⁻¹². One way to distinguish the TIs belonging to different orders is through their edge states. For example, a Chern insulator, which is a type of first-order TIs characterized by the Chern number or quantized Hall conductance, has gapless chiral states at its edge. On the other hand, the edge states are still gapped for a second-order TI in two dimensions. However, if the boundaries of the sample are compatible with the protecting symmetry, then gapless states will exist at the corners. The robustness of these gapless corner states is guaranteed by the second-order bulk topology.

Recently, the notion of higher-order topology has been extended to the Dirac semimetals (DSMs)¹³⁻¹⁵ as well as WSMs^{16,17}. A Dirac point in three dimensions can be understood as two degenerate Weyl nodes with opposite monopole charges, where crystalline symmetries

forbid the two Weyl nodes from hybridizing and opening a gap at each Dirac point¹⁸. Given this picture of the bulk, a three-dimensional (3D) DSM has two copies of arc-like surface states which resemble Fermi-arcs in WSMs, i.e., the double Fermi arcs. However, unlike the surface states in the WSM, the double Fermi arcs on the surface of a DSM are not topologically protected. They can be continuously deformed into a closed Fermi contour without any symmetry breaking or bulk phase transition¹⁹. Therefore, they are not topological consequences of the bulk Dirac points themselves. In contrast, the higher-order DSMs (HODSMs) can exhibit robust and nontrivial topology with spectroscopic consequences. It has been proposed that the HODSM can be realized in the room- (α) and intermediate-temperature (α'') phases of Cd_3As_2 , KMgBi , and rutile structure (β' -) PbO_2 ^{20,21}.

The minimal model of HODSMs contains a pair of Dirac points located at the same energy. For simplicity, we take the two Dirac points at the crystal momenta $\pm\mathbf{K}$ where $\mathbf{K} = (0, 0, k_0)$ with $0 < k_0 < \pi$ (by setting the lattice constant to be unit). Each plane with given $k_z \neq \pm k_0$ in the first BZ describes the band structure of a two-dimensional (2D) insulator. The two planes at $k_z = \pm k_0$ then separate the first BZ into two regions, each consisting of 2D insulators by treating k_z as a free parameter. In a second-order DSM, one of the regions consists of 2D second-order TIs, while the other consists of trivial insulators. For a cubic sample with open boundary conditions in both the x and y directions and periodic boundary conditions in the z direction, each 2D second-order TI will host gapless states at its corners. (That is, the energy of the corner states coincides with that of the Dirac points.) Hence, these gapless corner states form Fermi arcs on the 1D hinges terminated at the projections of the two Dirac points. It is clear that these Fermi arcs are direct, topological consequences of the bulk Dirac points, in contrast with the first-order DSM.

In the present work, we study the effects of the long range Coulomb interaction on a second-order DSM. The Coulomb interaction is ubiquitous in condensed matter systems. Especially, its long range nature remains intact in semimetals, in contrast with the Fermi liquid. For the 3D first-order DSM at weak coupling, one-loop renormalization group (RG) analysis indicates that the Fermi velocity grows to infinity logarithmically at low energies, leading to the marginally irrelevant dimensionless coupling constant^{22–24}. For the second-order DSM, the full rotation symmetry is lost even in the continuum limit, and thus the low-energy physics is described by two parameters: the dimensionless coupling constant and the ratio of the anisotropy parameters. We employ the method of RG and show that the coupling constant flows to zero at low energies, similar to the first-order DSM, where as the ratio of the anisotropy parameters flows to a fixed value at low energies. To illustrate the effects of the Coulomb interaction, we calculate the temperature dependence of the specific heat in terms of the RG equations. We find that in comparison with the specific heat of a non-interacting second-order DSM, the Coulomb interaction suppresses its value at all temperatures, except at zero temperature and the temperature close to the band width.

The breaking of the full rotation symmetry introduces a crossover temperature scale T_c (and thus a characteristic length scale L_c). When the temperature is smaller than T_c , the values of physical quantities are expected to approach the ones for a first-order DSM. However, we find that this expectation is realized only at extremely low temperatures or long distances. We illustrate this point by the temperature dependence of the specific heat and the momentum dependence of the screened Coulomb potential within the RPA approximation.

The rest of the work is organized as follows. We introduce the model of the second-order DSM in Sec. II. The results of the RPA approximation and the one-loop RG are presented in Sec. III and IV, respectively. The last section is our conclusions. The details of the calculations are shown in two appendices.

II. THE MODEL

A. The Hamiltonian

We start with a lattice model describing the second-order DSM. Its Bloch Hamiltonian is written as $H(\mathbf{k}) = H_0(\mathbf{k}) + H_1(\mathbf{k})$ where^{14,15}

$$\begin{aligned} H_0(\mathbf{k}) &= t \sum_{j=1,2} S_j \Gamma_j - t_3 \left[C_3 + \sum_{j=1,2} (1 - C_j) \right] \Gamma_3, \\ H_1(\mathbf{k}) &= t_1 [(C_1 - C_2) \Gamma_4 + S_1 S_2 \Gamma_5]. \end{aligned} \quad (1)$$

Here $C_j = \cos(k_j a_0)$, $S_j = \sin(k_j a_0)$, a_0 is the lattice constant, and $\mathbf{k} = (k_1, k_2, k_3)$. The five rank-4 Γ matrices

take the forms $\Gamma_1 = \tau_1 \otimes \sigma_3$, $\Gamma_2 = \tau_2 \otimes \sigma_0$, $\Gamma_3 = \tau_3 \otimes \sigma_0$, $\Gamma_4 = \tau_1 \otimes \sigma_1$, and $\Gamma_5 = \tau_1 \otimes \sigma_2$. One may verify that they are all Hermitian and satisfy the Clifford algebra

$$\{\Gamma_i, \Gamma_j\} = 2\delta_{ij}, \quad (2)$$

for $i, j = 1, \dots, 5$. Here σ_μ and τ_μ with $\mu = 0, 1, 2, 3$ are the standard Pauli matrices acting on the spin and orbital spaces, respectively.

In this model, the two orbitals are the eigenstates of the space inversion $\hat{P} = \tau_3 \otimes \sigma_0$. On the other hand, the time reversal is implemented by the usual one for spin-1/2 fermions, i.e., $\hat{T} = \tau_0 \otimes (i\sigma_2)\mathcal{K}$ where \mathcal{K} takes the complex conjugation. It is straightforward to verify that $H_0(\mathbf{k})$ preserves both the space inversion (P) and time-reversal (T) symmetries, while $H_1(\mathbf{k})$ breaks both symmetries. However, $H(\mathbf{k})$ has a PT symmetry, i.e.,

$$\hat{\Theta} H(\mathbf{k}) \hat{\Theta}^{-1} = H(\mathbf{k}), \quad (3)$$

where $\hat{\Theta} \equiv \hat{P}\hat{T}$. Note that $\hat{\Theta}^2 = -1$. Therefore, this symmetry assures that each energy level labeled by \mathbf{k} is doubly degenerate.

The band structure is given by $E_\pm(\mathbf{k}) = \pm E(\mathbf{k})$ where

$$E(\mathbf{k}) = \sqrt{\sum_{j=1}^5 [g_j(\mathbf{k})]^2}, \quad (4)$$

where $g_1(\mathbf{k}) = tS_1$, $g_2(\mathbf{k}) = tS_2$, $g_3(\mathbf{k}) = -t_3(C_3 + 2 - C_1 - C_2)$, $g_4(\mathbf{k}) = t_1(C_1 - C_2)$, and $g_5(\mathbf{k}) = t_1 S_1 S_2$. Each band is two-fold degenerate, as required by the PT symmetry. The upper and lower bands touch each other at the points where $E(\mathbf{k}) = 0$ or $g_j(\mathbf{k}) = 0$ for $j = 1, \dots, 5$, which are the Dirac points. In this case, the Dirac points are located at $\pm \mathbf{K}$ where $\mathbf{K} = (0, 0, \pi/2)$ ²⁵. Notice that the locations of the Dirac points are not affected by $H_1(\mathbf{k})$.

When the Fermi level coincides with the energy at the Dirac points, i.e., $\mu = 0$, then the low-energy effective Hamiltonian can be obtained by expanding around the two Dirac points, yielding

$$H_{eff}(\mathbf{p}) = \tilde{h}_+(\mathbf{p}) + \tilde{h}_-(\mathbf{p}), \quad (5)$$

to the leading terms in \mathbf{p} , where $\mathbf{k} = \pm \mathbf{K} + \mathbf{p}$ and

$$\tilde{h}_\pm(\mathbf{p}) = v_\perp \sum_{j=1,2} p_j \Gamma_j \pm v_3 p_3 \Gamma_3 + b \sum_{j=4,5} d_j(\mathbf{p}) \Gamma_j, \quad (6)$$

with $v_\perp = ta_0$, $v_3 = t_3 a_0$, $b = t_1 a_0^2/2$, $d_4(\mathbf{p}) = p_2^2 - p_1^2$, and $d_5(\mathbf{p}) = 2p_1 p_2$. Note that $H_{eff}(\mathbf{p})$ and $H(\mathbf{k})$ share the same symmetries. Moreover, $b = 0$ and $b \neq 0$ correspond to the first-order and second-order DSMs, respectively²⁶.

Now we add the Coulomb interaction to the system. The low-energy effective Hamiltonian around the two Dirac nodes $\pm \mathbf{K}$ are given by

$$H = \sum_{\xi=\pm} \int d^3x \psi_\xi^\dagger h_\xi \psi_\xi + H_c, \quad (7)$$

where h_ξ is the inverse Fourier transform of $\tilde{h}_\xi(\mathbf{p})$ and

$$H_c = \frac{1}{2} \int d^3x d^3y \rho_0(\mathbf{x}) V_c(|\mathbf{x} - \mathbf{y}|) \rho_0(\mathbf{y}). \quad (8)$$

Here ξ is the node index, ψ_ξ and ψ_ξ^\dagger obey the canonical anticommutation relations, $\rho_0(\mathbf{r}) = \sum_\xi \psi_\xi^\dagger \psi_\xi(\mathbf{r})$ is the uniform component of the electron density, and $V_c(\mathbf{r}) = e^2/(4\pi\epsilon r)$ with the dielectric constant ϵ .

The action in the imaginary-time formulation is then of the form

$$S = \sum_{\xi=\pm} \int_X \psi_\xi^\dagger (\partial_\tau + h_\xi) \psi_\xi + i \int_X \phi \rho_0 + \frac{1}{2} \int_X \left[\frac{1}{g_\perp^2} |\nabla_\perp \phi|^2 + \frac{1}{g_3^2} |\partial_3 \phi|^2 \right], \quad (9)$$

where $X = (\tau, \mathbf{r})$, $\int_X = \int d\tau d^3x$, $\nabla_\perp = (\partial_1, \partial_2)$, and $g_\perp^2 = g_3^2 = g^2 = e^2/\epsilon$. We have introduced a real bosonic field ϕ to describe the Coulomb interaction. As usual, the full rotation symmetry is recovered in the continuum limit. In the present case, it is not the case when $b \neq 0$ even if we set $v_\perp = v_3$. As a result, the longitudinal and transverse components of $|\nabla\phi|^2$ will acquire different renormalization. Hence, we introduce different coupling constants g_\perp^2 and g_3^2 though they have the same bare value.

B. The specific heat of the non-interacting DSM

In the present case, one consequence of the breaking of the full rotation symmetry is the introduction of a crossover temperature T_c . To show this, we first compute the specific heat for the non-interacting second-order DSM.

For the non-interacting second-order DSM, the specific heat is given by

$$c_v(T) = \frac{T^3}{2v_\perp^2 v_3 \pi^2} \int_0^{+\infty} dx \frac{g(Tx/T_c) x^4 e^{-x}}{(1 + e^{-x})^2}, \quad (10)$$

where $T_c = v_\perp^2/|b|$ and

$$g(x) = \frac{1}{\sqrt{|x|}} \int_{w(x)}^1 \frac{dt}{\sqrt{1-t} \sqrt{|x|t - \sqrt{1-t}}},$$

$$w(x) = \frac{2}{\sqrt{1+4x^2+1}}.$$

The function $g(x)$ is in a certain sense a measure of the density of states (DOS) for the second-order DSM since the latter can be written as

$$\rho(\epsilon) = \frac{g(\epsilon/T_c) \epsilon^2}{4v_\perp^2 v_3 \pi^2}.$$

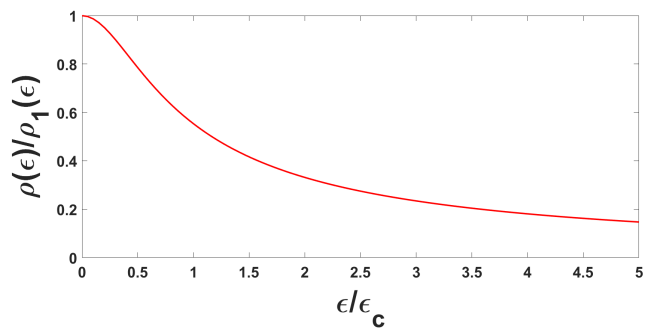


FIG. 1: The DOS $\rho(\epsilon)$ as a function of ϵ . We measure $\rho(\epsilon)$ in units of $\rho_1(\epsilon)$, the DOS for the non-interacting first-order DSM, and ϵ in units of $\epsilon_c = T_c$.

When $T \ll T_c$, $g(x) \approx 4$ and we find that $\rho(\epsilon) \approx \rho_1(\epsilon) = \epsilon^2/(v_\perp^2 v_3 \pi^2)$, which is the DOS for the first-order DSM, and

$$c_v(T) \approx c_1(T) \equiv \frac{7\pi^2 T^3}{15v_\perp^2 v_3}, \quad (11)$$

which is the specific heat of the first-order DSM.

Figure 1 shows the DOS for the non-interacting second-order DSM. We see that it approaches the one for the non-interacting first-order DSM only at extremely low energies. $b \neq 0$ suppresses the value of $\rho(\epsilon)$ compared with the one for the non-interacting first-order DSM. Following from this fact, in the most temperature range, the thermodynamic properties of a second-order DSM will deviate significantly from those of a first-order DSM.

III. THE RPA APPROXIMATION

There exists a characteristic length scale L_c associated with the crossover temperature T_c introduced by b . The momentum or position dependence of a physical quantity will depend on L_c in a nontrivial way. To illustrate this point, we consider the screened Coulomb potential. In the momentum space, its Fourier transform $\mathcal{V}_s(\mathbf{q})$ satisfies the Dyson equation

$$\frac{1}{\mathcal{V}_s(\mathbf{q})} = \frac{1}{\mathcal{V}_0(\mathbf{q})} + \Pi(0, \mathbf{q}), \quad (12)$$

where $\mathcal{V}_0(\mathbf{q}) = g^2/\mathbf{q}^2$ is the Fourier transform of the bare Coulomb potential $V_c(\mathbf{r})$ and $\Pi(0, \mathbf{q})$ is the vacuum polarization at zero frequency.

Within the RPA approximation, the vacuum polarization is given by

$$\Pi(Q) = -\frac{1}{v_\perp^2 v_3} \sum_\xi \int' \frac{d^3\tilde{p}}{(2\pi)^3} \int_{-\infty}^{+\infty} \frac{dp_0}{2\pi} \text{tr}[G_{\xi 0}(P) G_{\xi 0}(P + Q)],$$

where $Q = (iq_0, \mathbf{q})$, $\tilde{p}_{1/2} = v_\perp p_{1/2}$, $\tilde{p}_3 = v_3 p_3$, $\tilde{b} = b/v_\perp^2$, $\tilde{\mathbf{p}}_\perp = (\tilde{p}_1, \tilde{p}_2)$, and

$$G_{\xi_0}(P) = \frac{ip_0 + \sum_{j=1,2} \tilde{p}_j \Gamma_j + \xi \tilde{p}_3 \Gamma_3 + \tilde{b} \sum_{j=4,5} d_j(\tilde{\mathbf{p}}_\perp) \Gamma_j}{p_0^2 + \tilde{\mathbf{p}}_\perp^2 + \tilde{p}_3^2 + \tilde{b}^2 \tilde{\mathbf{p}}_\perp^4},$$

is the free propagator of the fermion fields. Due to the complicated form of $\Pi(0, \mathbf{q})$, we will evaluate it in two situations: (i) $\mathbf{q}_\perp = 0$ and $q_3 \neq 0$ and (ii) $\mathbf{q}_\perp \neq 0$ and $q_3 = 0$. We just present the results and discuss their consequences. The details of calculations are left to appendix A.

For case (i), we find that

$$\Pi(0, 0, q_3) = \frac{\tilde{q}_3^2}{v_\perp^2 v_3 \pi^2} I_3(\tilde{b} \tilde{q}_3), \quad (13)$$

where $\tilde{q}_3 = v_3 q_3$,

$$I_3(x) = \int_0^{+\infty} ds \left(1 - \frac{[\tilde{a}(s, x)]^2 - 1}{2\tilde{a}(s, x)} \ln \left| \frac{\tilde{a}(s, x) + 1}{\tilde{a}(s, x) - 1} \right| \right),$$

and

$$\tilde{a}(s, x) = \sqrt{1 + 4s + 4x^2 s^2}.$$

We plot the function $I_3(x)$ in Fig. 2. One may obtain the asymptotic behaviors of it in the limits $|x| \ll 1$ and $|x| \gg 1$:

$$I_3(x) = \begin{cases} -\frac{1}{3} \ln |x| & |x| \ll 1 \\ \frac{\pi^2}{16|x|} & |x| \gg 1 \end{cases}.$$

Thus, in the limit $|\tilde{b} \tilde{q}_3| = L_c |q_3| \ll 1$, we find that

$$\Pi(0, 0, q_3) \approx -\frac{\tilde{q}_3^2}{3v_\perp^2 v_3 \pi^2} \ln |\tilde{b} \tilde{q}_3| = -\frac{v_3 q_3^2}{3v_\perp^2 \pi^2} \ln(L_c |q_3|), \quad (14)$$

and

$$\Pi(0, 0, q_3) \approx \frac{|\tilde{q}_3|}{16|\tilde{b}|v_\perp^2 v_3} = \frac{v_3 |q_3|}{16L_c v_\perp^2}, \quad (15)$$

for $|\tilde{b} \tilde{q}_3| = L_c |q_3| \gg 1$, where $L_c = v_3 |b|/v_\perp^2 = v_3/T_c$.

For case (ii), we find that

$$\Pi(0, \mathbf{q}_\perp, 0) = \frac{\tilde{q}_\perp^2}{3v_\perp^2 v_3 \pi^2} \ln \left(\frac{\Lambda}{\mu} \right) + \dots,$$

when $|\tilde{b} \tilde{q}_\perp| \ll 1$, and

$$\Pi(0, \mathbf{q}_\perp, 0) \approx \frac{4\tilde{q}_\perp^2}{3v_\perp^2 v_3 \pi^2} \ln \left(\frac{\Lambda}{\mu} \right) + \dots,$$

when $|\tilde{b} \tilde{q}_\perp| \gg 1$, where $\tilde{q}_{1/2} = v_\perp q_{1/2}$, $\tilde{\mathbf{q}}_\perp = (\tilde{q}_1, \tilde{q}_2)$, Λ is an UV cutoff in $|\tilde{\mathbf{p}}_\perp|$, μ is an IR energy scale, and \dots denotes the finite part. In the above calculation for the

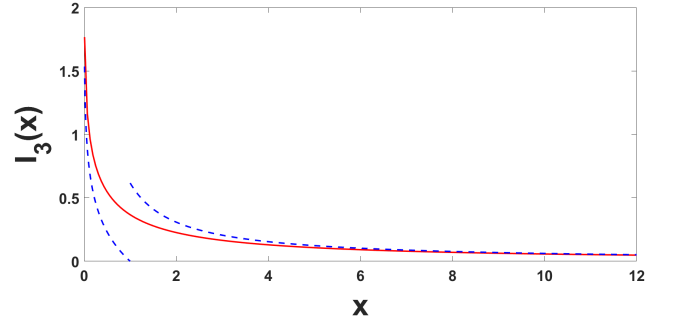


FIG. 2: The plot of the function $I_3(x)$ (solid line). The dashed line is the plot of the function $-\ln|x|/3$ and $\pi^2/(16|x|)$ for $|x| < 1$ and $|x| > 1$, respectively.

momentum integrals, we follow the strategy employed in Ref. 6 and integrate $\tilde{\mathbf{p}}_\perp$ and \tilde{p}_3 over the ranges $0 < |\tilde{\mathbf{p}}_\perp| < \Lambda$ and $-\infty < \tilde{p}_3 < +\infty$, respectively.

We see that the leading behaviors in $\Pi(0, \mathbf{q}_\perp, 0) \sim q_\perp^2$ in both regimes $q_\perp \ll 1/L_c$ and $q_\perp \gg 1/L_c$. The logarithmic divergence in front of the q_\perp^2 term can be absorbed into g^2 , leading to the (infinite) renormalization of the coupling constant g^2 within the RPA (or large N) approximation. (If we replace ψ_ξ by $\psi_{\xi\beta}$ with $\beta = 1, 2, \dots, N$, then the RPA result is exact in the large N limit.) The regimes $q_\perp \ll 1/L_c$ and $q_\perp \gg 1/L_c$ correspond to the first-order and second-order DSMs, respectively. Therefore, the different coefficients in front of $q_\perp^2 \ln(\Lambda/\mu)$ imply different renormalization of g^2 in both regimes.

In view of Eq. (12), the coupling constant $g_\perp^2(\mu)$ at the scale μ can be defined as

$$\frac{1}{g_\perp^2(\mu)} = \frac{1}{g_\perp^2(\Lambda)} + \frac{c}{3v_3 \pi^2} \ln \left(\frac{\Lambda}{\mu} \right),$$

where $c = 1, 4$ for $q_\perp \ll 1/L_c$ and $q_\perp \gg 1/L_c$, respectively. Thus, we find that

$$\Lambda \frac{\partial \alpha}{\partial \Lambda} = \frac{4c}{3} \alpha^2, \quad (16)$$

where $\alpha = g_\perp^2/(4\pi^2 v_3)$ is the dimensionless coupling constant. Equation (16) indicates that α flows to zero at low energies. Accordingly, the DSM is stable against the presence of the Coulomb interaction in the large N limit.

The above analysis suggests the following behavior for $\mathcal{V}_s(\mathbf{q})$. It acquires only a logarithmic correction at small momenta, as in the case of the first-order DSM. On the other hand, for $q \gg 1/L_c$,

$$\mathcal{V}_s(\mathbf{q}) \approx \frac{g^2}{q^2 + w|q_3|},$$

where $w > 0$ is a nonuniversal constant. Within the RPA approximation, we get $w = v_3 g^2/(16L_c v_\perp^2)$. When L_c is very large, the screened Coulomb potential in the real

space is approximately given by

$$V_s(\mathbf{r}) \approx \int \frac{d^3p}{(2\pi)^3} e^{i\mathbf{p}\cdot\mathbf{r}} \frac{g^2}{\mathbf{p}^2 + w|p_3|} ,$$

except its tail. By performing the momentum integral, we find that

$$V_s(\mathbf{r}_\perp, 0) = \begin{cases} \frac{g^2}{8\pi^2 r_\perp} & r_\perp \ll 1/w \\ \frac{g^2}{2\pi^3 w r_\perp^2} & r_\perp \gg 1/w \end{cases} , \quad (17)$$

where $\mathbf{r}_\perp = (x, y)$ and

$$V_s(0, z) \approx \frac{g^2}{4\pi c|z|} , \quad (18)$$

for both $|z| \ll 1/w$ and $|z| \gg 1/w$, and $c = 1, 2$ when $|z| \ll 1/w$ and $|z| \gg 1/w$, respectively. (The details of the calculations are left to appendix A.) Therefore, if we place a charged impurity at the origin, the induced charge density $\rho_{ind}(\mathbf{r})$ will be anisotropic in the intermediate distance, while its tail ($r \gg L_c$) is approximately isotropic as in the case of the first-order DSM.

IV. THE RENORMALIZATION GROUP

A. One-loop RG equations

Now we study the effects of the Coulomb interaction in terms of the RG. To perform the RG transformation, we decompose each field into the slow and fast modes: $\psi_\xi = \psi_{\xi<} + \psi_{\xi>}$ and $\phi = \phi_{<} + \phi_{>}$ where the subscripts $<$ and $>$ denote the slow and fast modes, respectively. Due to the lack of the full rotation symmetry, we adopt the regularization scheme employed in the anisotropic Weyl fermions⁶ and double WSMs^{27,28}. That is, the fast modes consist of the Fourier components between the cylindrical shell $\Lambda/s < |\tilde{\mathbf{p}}_\perp| < \Lambda$ and $|\tilde{p}_3| < +\infty$ where $s = e^l > 1$.

Now we integrate out the fast modes to the one-loop order, and then perform the scaling transformation

$$\begin{aligned} x(y) &\rightarrow e^l x(y) , \quad z \rightarrow e^{z_3 l} z , \quad \tau \rightarrow e^{z_l \tau} , \\ \psi_{\xi<} &= Z_\psi^{-1/2} \psi_\xi , \quad \phi_{<} = Z_\phi^{-1/2} \phi . \end{aligned}$$

Note that the z - and transverse directions may have different scaling exponents on account of the breaking of the full rotation symmetry. The wavefunction renormalization constants Z_ψ and Z_ϕ are chosen to bring the terms $\int_X \psi_{\xi<}^\dagger \partial_\tau \psi_{\xi<}$ and $i \int_X \phi_{<} \rho_{0<}$ in the action back to their original forms. In this way, we obtain an effective action for the slow modes, which has the same form as S [Eq. (9)] but with renormalized parameters.

We further choose the values of z and z_3 such that v_3 and b are both RG invariants, yielding

$$z = 2 - \beta^3 \alpha G_4(\beta, \delta) , \quad z_3 = z + \beta \alpha G_3(\beta, \delta) , \quad (19)$$

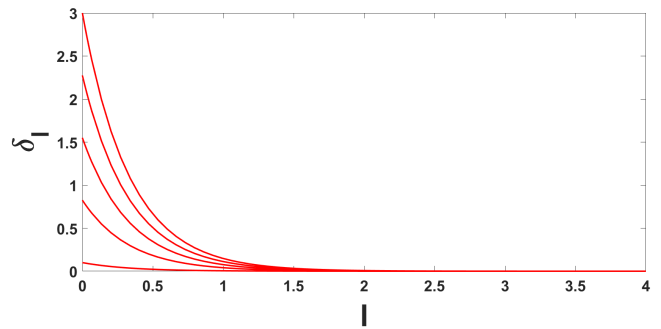


FIG. 3: The RG flow of δ with $\alpha_0 = 0.1$ and $\beta_0 = 0.3$.

where $r = v_\perp/v_3$ is the ratio of the components of the velocity, $\eta \equiv g_3^2/g_\perp^2$ is the anisotropy parameter, $\beta = \eta/r^2$, and $\delta = \tilde{b}\Lambda$. Therefore, the one-loop RG equations for these dimensionless parameters are given by

$$\frac{dr_l}{dl} = r_l + r_l \beta_l^2 \alpha_l [G_\perp(\beta_l, \delta_l) - \beta_l G_4(\beta_l, \delta_l)] , \quad (20)$$

$$\frac{d\delta_l}{dl} = -3\delta_l - 2\beta_l^2 \alpha_l \delta_l [G_\perp(\beta_l, \delta_l) - \beta_l G_4(\beta_l, \delta_l)] , \quad (21)$$

$$\frac{d\alpha_l}{dl} = -\alpha_l^2 [\beta_l G_3(\beta_l, \delta_l) + 2F_\perp(\delta_l)] , \quad (22)$$

$$\begin{aligned} \frac{d\beta_l}{dl} &= 2\beta_l^2 \alpha_l [G_3(\beta_l, \delta_l) - \beta_l G_\perp(\beta_l, \delta_l)] \\ &\quad + 2\beta_l \alpha_l [F_\perp(\delta_l) - \beta_l F_3(\delta_l)] , \end{aligned} \quad (23)$$

where A_l is the value of A at the scale l . In the above,

$$F_3(z) = \frac{2}{3(1+z^2)} , \quad F_\perp(z) = \frac{2+11z^2+8z^4}{3(1+z^2)^2} ,$$

and

$$\begin{aligned} G_\perp(\beta, z) &= \int_0^{+\infty} \frac{dt}{(t^2 + \beta)^2 \sqrt{t^2 + 1 + z^2}} , \\ G_3(\beta, z) &= \int_0^{+\infty} \frac{2t^2}{(t^2 + \beta)^2 \sqrt{t^2 + 1 + z^2}} dt , \\ G_4(\beta, z) &= \int_0^{+\infty} \frac{t}{(t^2 + \beta)^3 \sqrt{t^2 + 1 + z^2}} dt . \end{aligned}$$

The details of the derivation of Eqs. (20) – (23) are left in appendix B.

Equations (21) – (23) themselves form a closed set under RG transformations. Because $F_3(0) = 2/3 = F_\perp(0)$ and $G_3(1, 0) = 2/3 = G_\perp(1, 0)$, this set of one-loop RG equations has two fixed points: $(\alpha, \beta, \delta) = (0, 0, 0)$ and $(0, 1, 0)$. Around the two fixed points, δ always flows to zero at low energies, and thus it is an irrelevant parameter in the sense of RG. (Figure 3 plots the RG flow of δ .)

The typical RG flows of α and β are depicted in Fig. 4. We see that α is marginally irrelevant and flows to zero at low energies. On the other hand, β flows to 1 at

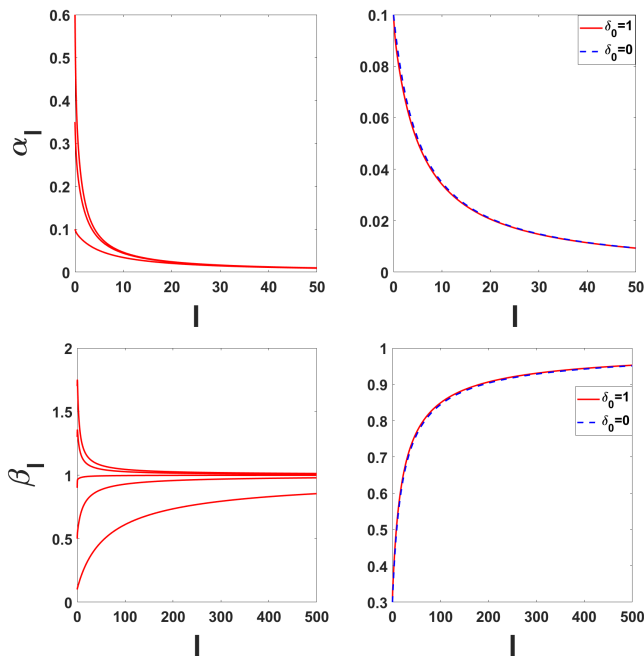


FIG. 4: **Top:** The RG flows of α with $\beta_0 = 0.3$, $\delta_0 = 1$, and different values of α_0 (left) and the RG flows of α with $\alpha_0 = 0.1$, $\beta_0 = 0.3$, and different values of δ_0 (right). **Bottom:** The RG flows of β with $\alpha_0 = 0.1$, $\delta_0 = 1$, and different values of β_0 (left) and the RG flows of β with $\alpha_0 = 0.1$, $\beta_0 = 0.3$, and different values of δ_0 (right). The curves for $\delta_0 \neq 0$ and $\delta_0 = 0$ almost coincide with each other due to the irrelevancy of δ under RG transformations.

low energies. These facts indicate that the fixed point $(\alpha, \beta, \delta) = (0, 0, 0)$ is IR unstable while the fixed point $(\alpha, \beta, \delta) = (0, 1, 0)$ is IR stable. It is the latter which controls the low-energy physics of the second-order DSM in the presence of long range Coulomb repulsion.

Since δ flows to zero quickly at low energies, we may set $\delta_l = 0$ in Eqs. (22) and (23), yielding

$$\frac{d\alpha_l}{dl} = -\alpha_l^2 \left[\beta_l G_3(\beta_l, 0) + \frac{4}{3} \right], \quad (24)$$

$$\begin{aligned} \frac{d\beta_l}{dl} &= 2\beta_l^2 \alpha_l [G_3(\beta_l, 0) - \beta_l G_\perp(\beta_l, 0)] \\ &\quad + \frac{4}{3} \beta_l \alpha_l (1 - \beta_l). \end{aligned} \quad (25)$$

Equations (24) and (25) correctly produce the RG flows of α and β , as illustrated in Fig. 4. We plot the flow diagram of α and β in Fig. 5 according to Eqs. (24) and (25), which reveals the nature of the two fixed points $(\alpha, \beta, \delta) = (0, 0, 0)$ and $(0, 1, 0)$. We see that β flows to 1 quickly under the RG transformations, so that the RG flow converges to the line $\beta = 1$. Along the surface $\beta_l = 1$ and $\delta_l = 0$, Eqs. (20) and (24) can be simplified and their solutions are

$$r_l = r_0 e^l (1 + 2\alpha_0 l)^{1/15}, \quad \alpha_l = \frac{\alpha_0}{1 + 2\alpha_0 l}, \quad (26)$$

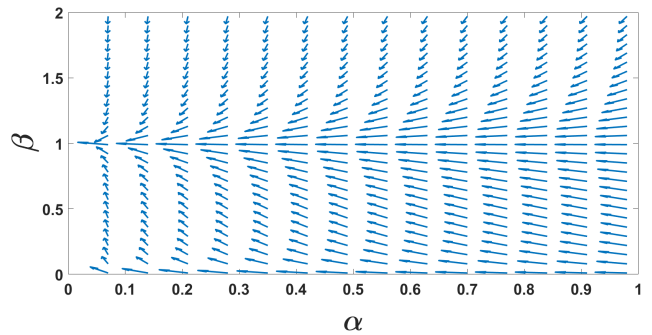


FIG. 5: The flow diagram of α and β . It is clear that the RG flow converges to the line $\beta = 1$.

respectively.

B. The specific heat of the interacting DSM

We are able to calculate the specific heat for the interacting DSM with the help of the RG equations^{28,31}. Let $f_l = f(T_l, r_l, v_{3l}, b_l, \alpha_l, \beta_l)$ be the free energy density at the scale l , which can be written as

$$f_l = -\frac{T_l}{V_l} \ln Z,$$

where Z is the partition function, and T_l , V_l are determined by the equations

$$\frac{dT_l}{dl} = zT_l, \quad (27)$$

and

$$\frac{dV_l}{dl} = -(2 + z_3)V_l,$$

with the initial conditions $T_0 = T$ and $V_0 = V$, respectively. Since we keep Z to be invariant under RG transformations, f_l satisfies the equation

$$\frac{df_l}{dl} = (2 + z_3 + z)f_l.$$

with the initial condition $f_0 = f$ where f is the free energy density of the system. We define c_l as

$$c_l = -T_l \frac{\partial^2 f_l}{\partial T_l^2}.$$

Then, c_l obeys the equation

$$\frac{dc_l}{dl} = (2 + z_3)c_l, \quad (28)$$

with the initial condition $c_0 = c_v$ where c_v is the specific heat of the system. We will run the RG transformation to the scale l_* such that $T_* = D$ where $A_* = A(l_*)$ and D is of the order of the band width.

According to the previous RG analysis, we have $v_{3*} = v_3$, $\beta_* \approx 1$, $b_* = b$, $\delta_* \approx 0$, and

$$z = 2 - \frac{8}{15}\alpha_l, \quad z_3 = 2 + \frac{2}{15}\alpha_l.$$

Inserting these into Eq. (27) and using Eq. (26), we get the solution of Eq. (27)

$$T_l = \frac{T e^{2l}}{(1 + 2\alpha_0 l)^{4/15}},$$

which results in

$$\frac{D}{T} = \frac{e^{2l_*}}{(1 + 2\alpha_0 l_*)^{4/15}}. \quad (29)$$

Equation (29) determines l_* as a function of T/D .

In terms of these results, the solution to Eq. (28) is

$$c_l = c_v e^{4l} (1 + 2\alpha_0 l)^{1/15},$$

which leads to

$$c_v = \frac{c_* e^{-4l_*}}{(1 + 2\alpha_0 l_*)^{1/15}}.$$

Here c_* is approximately given by the specific heat of a non-interacting DSM at temperature $T_* = D$, with v_\perp replaced by $v_{\perp*} = v_3 r_*$.

With the help of Eqs. (10) and (29), we get c_v for the second-order DSM

$$c_v(T) = \frac{T^3}{2v_\perp^2 v_3 \pi^2 (1 + 2\alpha_0 l_*)} \times \int_0^{+\infty} dx \frac{g(Tx/[T_c f(T)]) x^4 e^{-x}}{(1 + e^{-x})^2}, \quad (30)$$

where $f(T) = (1 + 2\alpha_0 l_*)^{2/5}$. The temperature dependence of c_v given by Eq. (30) is shown in Fig. 6, by assuming that $T_c \ll D$. We measure c_v in units of c_0 where $c_0 = c_1(T_c)$ is the specific heat of the first-order DSM at $T = T_c$.

A few points should be emphasized. (i) First of all, the value of c_v is suppressed in the presence of the Coulomb interaction when $T \ll D$. However, it approaches the one for a non-interacting second-order DSM at high temperatures, as it should be. (ii) Next, as shown in the inset, even in the absence of the Coulomb interaction, the value of c_v is close to the one for a non-interacting first-order DSM only at extremely low temperatures. In the presence of the Coulomb interaction, the deviation is more significant.

V. CONCLUSIONS

We have studied the effects of Coulomb interactions on a second-order DSM. In contrast with the first-order DSM, the full rotation symmetry is broken so that the

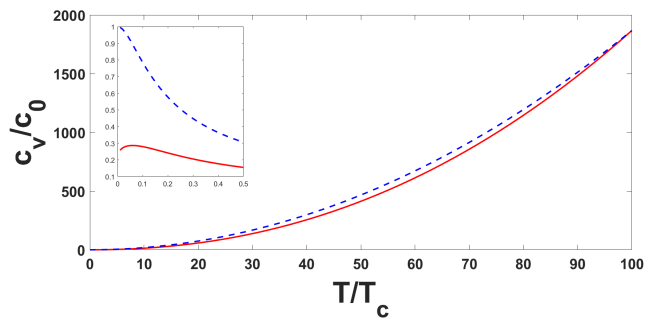


FIG. 6: c_v/c_0 as a function of T/T_c with $\alpha_0 = 0.3$ and $T_c/D = 0.01$, where c_0 is the specific heat of the first-order DSM at $T = T_c$. The solid and dashed lines correspond to the cases with and without the Coulomb interaction, respectively. The inset shows c_v , in units of the specific heat for a non-interacting first-order DSM, for $T/T_c < 0.5$.

low-energy physics is controlled by two dimensionless parameters: the dimensionless coupling constant α and the ratio of anisotropy parameters β . In terms of the one-loop RG equations, we show that α is marginally irrelevant and β flows to 1 at low energies. Therefore, physical quantities at low temperatures can be computed in terms of a renormalized perturbative expansion in α . As an application, we calculate the specific heat in terms of the RG. We find that the presence of the Coulomb interaction suppresses the value of specific heat, compared to the one for a non-interacting second-order DSM.

Another consequence following from the breaking of the full rotation symmetry is the existence of a crossover temperature T_c and an associated length scale L_c . When $T \ll T_c$, the values of physical quantities will be close to those for the first-order DSM; otherwise significant deviations will be observed. Similar phenomena will occur in the spatial dependence of the charge density produced by a charged impurity. When the distance r from the impurity is smaller than L_c , the induced charge density will be anisotropic. On the other hand, the tail of the induced charge density is isotropic.

In the present work, we derive the RG equation for the coupling constant within two different regimes: the large N limit [Eq. (16)] and the perturbative expansion to the one-loop order [Eq. (22)]. In both cases, the (dimensionless) coupling constant flows to zero at low energies. Therefore, the stability of the second-order DSM in the presence of the Coulomb interaction may go beyond the weak-coupling regime.

If we set $b = 0$, the Hamiltonian of the second-order DSM will reduce to the one of the first-order DSM. This corresponds to the limit $T_c \rightarrow +\infty$ or $L_c \rightarrow 0$. Our results become those for the first-order DSM in this limit. On the other hand, if we consider the highly anisotropic limit, i.e., $v_\perp = 0$, the Hamiltonian of the second-order DSM will be similar to that of a double WSM, except that the 2×2 Pauli matrices in the double WSM are

replaced the 4×4 Γ matrices in the present case. This corresponds to the limit $T_c \rightarrow 0$ or $L_c \rightarrow +\infty$. In fact, the functional form of the vacuum polarization in this limit is identical to that for a double WSM^{27,28}.

Most of our results are based on the one-loop RG equations, which hold only in the weak coupling regime. At strong coupling, the DSM may become unstable toward other phases. For the first-order DSM, it has been shown that the phase diagram may depend on the number N of the species of the Dirac fermions^{29,30}. Based on a U(1) lattice gauge theory with $N = 4$, a Mott insulating phase is identified when the Coulomb interaction becomes strong²⁹. By combining the RG method and the self-consistent resolution of Schwinger-Dyson equations, the strong Coulomb interaction results in dynamical mass generation for $N \leq 4$ and a line of critical points characterized by the suppression of the quasiparticle weight at low energies for $N \gg 1$ ³⁰. It is interesting to see whether

or not similar phenomena will occur for the second-order DSM.

Acknowledgments

The works of Y.-W. Lee and Y.L. Lee are supported by the Ministry of Science and Technology, Taiwan, under the grant number MOST 109-2112-M-029-004 and MOST 109-2112-M-018-006, respectively.

Appendix A: The vacuum polarization

Here we present the details of the calculation for the vacuum polarization. Performing the trace over the Γ matrices, we find that

$$\begin{aligned} \Pi(0, 0, q_3) &= \frac{8}{v_\perp^2 v_3} \int' \frac{d^3 \tilde{p}}{(2\pi)^3} \int_{-\infty}^{+\infty} \frac{dp_0}{2\pi} \frac{p_0^2 - \tilde{p}_3(\tilde{p}_3 + \tilde{q}_3) - \tilde{p}_\perp^2 - \tilde{b}^2 \tilde{p}_\perp^4}{(p_0^2 + \tilde{p}_3^2 + \tilde{p}_\perp^2 + \tilde{b}^2 \tilde{p}_\perp^4)[p_0^2 + (\tilde{p}_3 + \tilde{q}_3)^2 + \tilde{p}_\perp^2 + \tilde{b}^2 \tilde{p}_\perp^4]} \\ &= \frac{8}{v_\perp^2 v_3} \int_0^1 dx \int' \frac{d^3 \tilde{p}}{(2\pi)^3} \int_{-\infty}^{+\infty} \frac{dp_0}{2\pi} \frac{p_0^2 - \tilde{p}_3(\tilde{p}_3 + \tilde{q}_3) - \tilde{p}_\perp^2 - \tilde{b}^2 \tilde{p}_\perp^4}{[p_0^2 + (\tilde{p}_3 + \tilde{q}_3 x)^2 + \tilde{p}_\perp^2 + \tilde{b}^2 \tilde{p}_\perp^4 + \tilde{q}_3^2 x(1-x)]^2} \\ &= \frac{2\tilde{q}_3^2}{v_\perp^2 v_3 \pi^2} \int_0^1 dx x(1-x) \int_0^\Lambda d\tilde{p}_\perp \frac{\tilde{p}_\perp}{\tilde{p}_\perp^2 + \tilde{b}^2 \tilde{p}_\perp^4 + \tilde{q}_3^2 x(1-x)}, \end{aligned}$$

and

$$\begin{aligned} \Pi(0, \mathbf{q}_\perp, 0) &= \frac{8}{v_\perp^2 v_3} \int' \frac{d^3 \tilde{p}}{(2\pi)^3} \int_{-\infty}^{+\infty} \frac{dp_0}{2\pi} \frac{p_0^2 - \tilde{p}_3^2 - \tilde{p}_\perp \cdot (\tilde{p}_\perp + \tilde{q}_\perp) - \tilde{b}^2 \sum_{j=4,5} d_j(\tilde{p}_\perp) d_j(\tilde{p}_\perp + \tilde{q}_\perp)}{(p_0^2 + \tilde{p}_3^2 + \tilde{p}_\perp^2 + \tilde{b}^2 \tilde{p}_\perp^4)[p_0^2 + \tilde{p}_3^2 + (\tilde{p}_\perp + \tilde{q}_\perp)^2 + \tilde{b}^2 (\tilde{p}_\perp + \tilde{q}_\perp)^4]} \\ &= \frac{8}{v_\perp^2 v_3} \int_0^1 dx \int' \frac{d^3 \tilde{p}}{(2\pi)^3} \int_{-\infty}^{+\infty} \frac{dp_0}{2\pi} \frac{p_0^2 - \tilde{p}_3^2 - \tilde{p}_\perp \cdot (\tilde{p}_\perp + \tilde{q}_\perp) - \tilde{b}^2 \sum_{j=4,5} d_j(\tilde{p}_\perp) d_j(\tilde{p}_\perp + \tilde{q}_\perp)}{\{p_0^2 + \tilde{p}_3^2 + (1-x)(\tilde{p}_\perp^2 + \tilde{b}^2 \tilde{p}_\perp^4) + x[(\tilde{p}_\perp + \tilde{q}_\perp)^2 + \tilde{b}^2 (\tilde{p}_\perp + \tilde{q}_\perp)^4]\}^2} \\ &= \frac{2}{v_\perp^2 v_3 \pi} \int_0^1 dx \int_\Lambda \frac{d\tilde{p}_1 d\tilde{p}_2}{(2\pi)^2} \left[1 - \frac{\tilde{p}_\perp \cdot (\tilde{p}_\perp + \tilde{q}_\perp) + \tilde{b}^2 (\tilde{p}_2^2 - \tilde{p}_1^2)[(\tilde{p}_2 + \tilde{q}_2)^2 - (\tilde{p}_1 + \tilde{q}_1)^2] + 4\tilde{b}^2 \tilde{p}_1 \tilde{p}_2 (\tilde{p}_1 + \tilde{q}_1)(\tilde{p}_2 + \tilde{q}_2)}{(1-x)(\tilde{p}_\perp^2 + \tilde{b}^2 \tilde{p}_\perp^4) + x[(\tilde{p}_\perp + \tilde{q}_\perp)^2 + \tilde{b}^2 (\tilde{p}_\perp + \tilde{q}_\perp)^4]} \right], \end{aligned}$$

where $\int' d^3 \tilde{p} = \int_{|\tilde{p}_\perp| < \Lambda} d\tilde{p}_1 d\tilde{p}_2 \int_{-\infty}^{+\infty} d\tilde{p}_3$. In the above, we have used the identity

$$\int_{-\infty}^{+\infty} dp_0 \frac{p_0^2 - \Delta^2}{(p_0^2 + \Delta^2)^2} = 0,$$

and the dimensional regularization to perform the integration over p_0 and \tilde{p}_3 . For the case with $\mathbf{q}_\perp = 0$ and $q_3 \neq 0$, we first perform the x integral, yielding Eq. (13).

For the case with $\mathbf{q}_\perp \neq 0$ and $q_3 = 0$, without loss of generality, we choose the coordinate frame such that $\tilde{\mathbf{q}}_\perp = (\tilde{q}_\perp, 0)$. Therefore, we have

$$\frac{\partial}{\partial \Lambda} \Pi(0, \mathbf{q}_\perp, 0) = \frac{\Lambda}{2v_\perp^2 v_3 \pi^2} I_\perp(t, \tilde{b}\tilde{q}_\perp),$$

where $t = \Lambda/\tilde{q}_\perp$ and

$$I_\perp(t, s) = \int_0^1 dx \int_0^{2\pi} \frac{d\phi}{\pi} \left[1 - \frac{t^2 + t \cos \phi + s^2 t^2 [\cos(2\phi) + 2t \cos \phi + t^2]}{(1-x)(t^2 + s^2 t^4) + x[1 + 2t \cos \phi + t^2 + s^2(1 + 2t \cos \phi + t^2)]} \right],$$

For $|s| \ll 1$, we have

$$I_{\perp}(t, s) \approx \int_0^1 dx \int_0^{2\pi} \frac{d\phi}{\pi} \left(1 - \frac{t + \cos \phi}{t + x/t + 2x \cos \phi} \right) = 2 - \int_0^1 \frac{dx}{x} \left[1 - \frac{(1 - 2t^2)x + t^2}{\sqrt{(1 - 4t^2)x^2 + 2t^2x + t^4}} \right].$$

Note that $t/x + 1/t > 2/x \geq 2$. When $t \gg 1$, this equation can be written as

$$I_{\perp}(t, s) = 2 - 2 \int_0^1 dx \left[1 - \frac{2x(1-x)}{t^2} \right] + O(1/t^4) = \frac{2}{3t^2} + O(1/t^4).$$

Thus, we find that

$$\Pi(0, \mathbf{q}_{\perp}, 0) \approx \frac{\tilde{q}_{\perp}^2}{3v_{\perp}^2 v_3 \pi^2} \int_{\mu/\tilde{q}_{\perp}}^{\Lambda/\tilde{q}_{\perp}} \frac{dt}{t} + \dots = \frac{\tilde{q}_{\perp}^2}{3v_{\perp}^2 v_3 \pi^2} \ln\left(\frac{\Lambda}{\mu}\right) + \dots,$$

when $|\tilde{b}|\tilde{q}_{\perp} \ll 1$, where μ is an IR energy scale and \dots denotes the finite part.

On the other hand, for $|s| \gg 1$, we have

$$I_{\perp}(t, s) \approx \int_0^1 dx \int_0^{2\pi} \frac{d\phi}{\pi} \left[1 - \frac{1 + (2/t) \cos \phi + (1/t^2) \cos(2\phi)}{1 + (4x/t) \cos \phi + (2x/t^2)(1 + 2 \cos^2 \phi) + (4x/t^3) \cos \phi + x/t^4} \right].$$

When $t \gg 1$, we find that

$$\begin{aligned} I_{\perp}(t, s) &\approx \frac{2}{t^2} \int_0^1 dx \int_0^{2\pi} \frac{d\phi}{\pi} [x + (6x - 8x^2) \cos^2 \phi] \\ &\quad + O(1/t^3) \\ &= \frac{8}{3t^2} + O(1/t^3), \end{aligned}$$

which leads to

$$\Pi(0, \mathbf{q}_{\perp}, 0) \approx \frac{4\tilde{q}_{\perp}^2}{3v_{\perp}^2 v_3 \pi^2} \ln\left(\frac{\Lambda}{\mu}\right) + \dots,$$

when $|\tilde{b}|\tilde{q}_{\perp} \gg 1$, where μ is an IR energy scale and \dots denotes the finite part.

These calculations suggest that the screened Coulomb potential $\mathcal{V}_s(\mathbf{q})$ in the momentum space takes the form

$$\mathcal{V}_s(\mathbf{q}) = \frac{g^2}{\mathbf{q}^2 + w|q_3|},$$

when $q \gg 1/L_c$. When L_c is very large, the screened Coulomb potential in the real space is approximately given by

$$V_s(\mathbf{r}) \approx \int d^3 q e^{i\mathbf{q}\cdot\mathbf{r}} \frac{g^2}{\mathbf{q}^2 + w|q_3|},$$

except its tail.

In the transverse direction, we have

$$\begin{aligned} V_s(\mathbf{r}_{\perp}, 0) &= g^2 \int_{-\infty}^{+\infty} \frac{dp_3}{2\pi} \int \frac{dp_1 dp_2}{(2\pi)^2} \frac{e^{i\mathbf{p}_{\perp}\cdot\mathbf{r}_{\perp}}}{\mathbf{p}_{\perp}^2 + p_3^2 + w|p_3|} \\ &= g^2 \int_{-\infty}^{+\infty} \frac{dp_3}{2\pi} \int_0^{+\infty} \frac{dp_{\perp} p_{\perp}}{(2\pi)^2} \int_0^{2\pi} d\theta \frac{e^{ip_{\perp} r_{\perp} \cos \theta}}{p_{\perp}^2 + p_3^2 + w|p_3|}, \end{aligned}$$

where $\mathbf{r}_{\perp} = (x, y)$ and $\mathbf{p}_{\perp} = (p_1, p_2)$. Using the Jacob-Auger expansion

$$e^{ip_{\perp} r_{\perp} \cos \theta} = \sum_{m=-\infty}^{+\infty} i^m e^{im\theta} J_m(p_{\perp} r_{\perp}),$$

where $J_m(x)$ is the Bessel function of order m , we find that

$$V_s(\mathbf{r}_{\perp}, 0) = g^2 \int_{-\infty}^{+\infty} \frac{dp_3}{2\pi} \int_0^{+\infty} \frac{dp_{\perp} p_{\perp}}{(2\pi)^2} \frac{J_0(p_{\perp} r_{\perp})}{p_{\perp}^2 + p_3^2 + w|p_3|}.$$

Integration over p_{\perp} can be done with the help of the identity³²

$$\int_0^{+\infty} dx \frac{x J_0(ax)}{x^2 + k^2} = K_0(ak),$$

where $a, k > 0$ and $K_0(z)$ is the modified Bessel function of the second kind of order 0, yielding

$$\begin{aligned} V_s(\mathbf{r}_{\perp}, 0) &= \frac{g^2}{4\pi^2} \int_{-\infty}^{+\infty} \frac{dp_3}{2\pi} K_0\left(\sqrt{p_3^2 + w|p_3|} r_{\perp}\right) \\ &= \frac{wg^2}{8\pi^3} \int_0^{+\infty} dt \frac{t}{\sqrt{t^2 + 1}} K_0(wr_{\perp} t/2) \\ &= \frac{g^2}{4\pi^3 r_{\perp}} \int_0^{+\infty} dt \frac{t}{\sqrt{t^2 + (wr_{\perp}/2)^2}} K_0(t). \end{aligned}$$

In terms of the identity³²

$$\int_0^{+\infty} dx x^{\mu} K_0(ax) = \frac{2^{\mu-1}}{a^{\mu+1}} \left[\Gamma\left(\frac{1+\mu}{2}\right) \right]^2,$$

where $\text{Re}(a) > 0$ and $\text{Re}(\mu + 1) > 0$, we get Eq. (17).

On the other hand, in the z direction, V_s is given by

$$\begin{aligned} V_s(0, z) &= g^2 \int \frac{dp_1 dp_2}{(2\pi)^2} \int_{-\infty}^{+\infty} \frac{dp_3}{2\pi} \frac{e^{ip_3 z}}{\mathbf{p}_\perp^2 + p_3^2 + w|p_3|} \\ &= g^2 \int \frac{dp_1 dp_2}{(2\pi)^2} \int_{-\infty}^{+\infty} \frac{dp_3}{2\pi} \frac{e^{ip_3 |z|}}{\mathbf{p}_\perp^2 + p_3^2 + w|p_3|} \\ &= \frac{g^2}{|z|} \int \frac{dp_1 dp_2}{(2\pi)^2} \int_{-\infty}^{+\infty} \frac{dt}{2\pi} \frac{e^{it}}{\mathbf{p}_\perp^2 + t^2 z^2 + w|z||t|} . \end{aligned}$$

For $w|z| \ll 1$, $V_s(0, z)$ can be approximated as

$$\begin{aligned} V_s(0, z) &\approx \frac{g^2}{|z|} \int \frac{dp_1 dp_2}{(2\pi)^2} \int_{-\infty}^{+\infty} \frac{dt}{2\pi} \frac{e^{it}}{\mathbf{p}_\perp^2 + t^2 z^2} \\ &= g^2 \int \frac{dp_1 dp_2}{(2\pi)^2} \int_{-\infty}^{+\infty} \frac{dp_3}{2\pi} \frac{e^{ip_3 |z|}}{\mathbf{p}_\perp^2 + p_3^2} \\ &= \frac{g^2}{2} \int \frac{dp_1 dp_2}{(2\pi)^2} \frac{e^{-p_\perp |z|}}{p_\perp} = \frac{g^2}{4\pi|z|} . \end{aligned}$$

For $w|z| \gg 1$, $V_s(0, z)$ can be approximated as

$$\begin{aligned} V_s(0, z) &\approx \frac{g^2}{|z|} \int \frac{dp_1 dp_2}{(2\pi)^2} \int_{-\infty}^{+\infty} \frac{dt}{2\pi} \frac{e^{it}}{\mathbf{p}_\perp^2 + w|z||t|} \\ &= g^2 \int \frac{dp_1 dp_2}{(2\pi)^2} \int_{-\infty}^{+\infty} \frac{dp_3}{2\pi} \frac{e^{ip_3 z}}{\mathbf{p}_\perp^2 + w|p_3|} \\ &= \frac{g^2}{\pi} \int \frac{dp_1 dp_2}{(2\pi)^2} \int_0^{+\infty} dp_3 \frac{\cos(p_3 |z|)}{\mathbf{p}_\perp^2 + wp_3} . \end{aligned}$$

The p_3 integral can be performed with the help of the identity³²

$$\int_0^{+\infty} dx \frac{\cos(ax)}{x + \beta} = -\sin(a\beta)\text{si}(a\beta) - \cos(a\beta)\text{ci}(a\beta) ,$$

where $a > 0$, $|\arg(\beta)| < \pi$, and $\text{si}(x)$, $\text{ci}(x)$ are respectively the sine and cosine integrals, yielding

$$\begin{aligned} V_s(0, z) &= -\frac{g^2}{4\pi^3 w} \int dp_1 dp_2 \sin(zp_\perp^2/w)\text{si}(zp_\perp^2/w) \\ &\quad -\frac{g^2}{4\pi^3 w} \int dp_1 dp_2 \cos(zp_\perp^2/w)\text{ci}(zp_\perp^2/w) \\ &= -\frac{g^2}{4\pi^2 w} \int_0^{+\infty} dt \sin(zt/w)\text{si}(zt/w) \\ &\quad -\frac{g^2}{4\pi^2 w} \int_0^{+\infty} dt \cos(zt/w)\text{ci}(zt/w) . \end{aligned}$$

Note that $\text{si}(-x) = -\text{si}(x)$ and $\text{ci}(-x) = \text{ci}(x)$. With the help of the identities³²

$$\begin{aligned} \int_0^{+\infty} dx \sin(px)\text{si}(qx) &= -\frac{\pi}{4p} \\ &= \int_0^{+\infty} dx \cos(px)\text{ci}(qx) , \end{aligned}$$

when $p^2 = q^2$, we find that

$$V_s(0, z) = \frac{g^2}{8\pi|z|} .$$

Appendix B: One-loop RG equations

By decomposing the fields into slow and fast modes, the action $S[\psi, \psi^\dagger, \phi]$ can be written as

$$S[\psi, \psi^\dagger, \phi] = S[\psi_<, \psi_<^\dagger, \phi_<] + S[\psi_>, \psi_>^\dagger, \phi_>] + S_{int} ,$$

where

$$S_{int} = i \sum_{\xi} \int_X \left[\phi_> (\psi_{\xi>}^\dagger \psi_{\xi<} + \psi_{\xi<}^\dagger \psi_{\xi>}) + \phi_< \psi_{\xi>}^\dagger \psi_{\xi>} \right] ,$$

describes the coupling between the slow and fast modes. Note that the terms with a single fast mode vanish due to momentum conservation. By integrating out the fast modes, we get an effective action for the slow modes

$$S_{eff}[\psi_<, \psi_<^\dagger, \phi_<] = S[\psi_<, \psi_<^\dagger, \phi_<] + I[\psi_<, \psi_<^\dagger, \phi_<] ,$$

where

$$\begin{aligned} e^{-I[\psi_<, \psi_<^\dagger, \phi_<]} &= \int D[\psi_>] D[\psi_>^\dagger] D[\phi_>] e^{-S[\psi_>, \psi_>^\dagger, \phi_>] - S_{int}} . \end{aligned}$$

In the following, we will compute I in terms of a perturbative expansion in powers of S_{int} .

Before plunging into the detailed calculations, we notice that the action S is invariant against the U(1) gauge transformation

$$\psi_\xi \rightarrow e^{-i\chi(\tau)} \psi_\xi , \quad \phi \rightarrow \phi + \partial_\tau \chi , \quad (\text{B1})$$

where χ is a function of the imaginary time τ . This gauge invariance results in a Ward identity, which puts a constraint on the low-energy physics. We now derive it.

By integrating out the fast modes, the action becomes

$$\begin{aligned} S &\rightarrow \sum_{\xi=\pm} \int_X \psi_\xi^\dagger [(1 + \Sigma_\tau) \partial_\tau + \bar{h}_\xi] \psi_\xi + (1 + \Gamma_v) i \int_X \phi \rho_0 \\ &\quad + \frac{1}{2} \int_X \left[\left(\frac{1}{g_\perp^2} + \Pi_\perp \right) |\nabla_\perp \phi|^2 + \left(\frac{1}{g_3^2} + \Pi_3 \right) |\partial_3 \phi|^2 \right] \\ &\quad + \dots , \end{aligned}$$

where \bar{h}_ξ is the renormalized Hamiltonian whose actual form is irrelevant to our discussion and \dots denotes the terms with higher scaling dimensions. The gauge invariance of S requires that

$$\Sigma_\tau = \Gamma_v . \quad (\text{B2})$$

Equation (B2) is the desired expression of the Ward identity.

To proceed, we write I as

$$I = \sum_{n=1}^{+\infty} I_n ,$$

where I_n denotes the contribution from S_{int}^n . We first compute I_1 which is given by

$$I_1 = \langle S_{int} \rangle = i \sum_{\xi} \int_X \phi_{<} \langle \psi_{\xi}^{\dagger} \psi_{\xi} \rangle ,$$

where $\langle \dots \rangle_{>}$ denotes the functional integral over the fast modes. Since

$$\begin{aligned} & \sum_{\xi} \langle \psi_{\xi}^{\dagger}(X) \psi_{\xi}(X) \rangle \\ &= \sum_{\xi} \int' \frac{d^3 p}{(2\pi)^3} \int_{-\infty}^{+\infty} \frac{dp_0}{2\pi} e^{ip_0 0^+} \text{tr}[G_{\xi 0}(P)] \\ &= -\frac{8}{v_{\perp}^2 v_3} \int' \frac{d^3 \tilde{p}}{(2\pi)^3} \int_{-\infty}^{+\infty} \frac{dp_0}{2\pi} \frac{ip_0}{p_0^2 + \tilde{\mathbf{p}}_{\perp}^2 + \tilde{p}_3^2 + \tilde{b}^2 \tilde{\mathbf{p}}_{\perp}^4} \\ &= 0 , \end{aligned}$$

we conclude that $I_1 = 0$.

Next, we calculate I_2 which is given by

$$I_2 = -\frac{1}{2} \langle S_{int}^2 \rangle + \frac{1}{2} I_1^2 = -\frac{1}{2} \langle S_{int}^2 \rangle .$$

In view of S_{int} , I_2 consists of two terms:

$$\begin{aligned} I_2 &= \sum_{\xi} \int_X \int_Y \psi_{\xi}^{\dagger}(X) \Sigma_{\xi}(X-Y) \psi_{\xi}(Y) \\ &\quad + \frac{1}{2} \int_X \int_Y \phi_{<}(X) \Pi(X-Y) \phi_{<}(Y) , \end{aligned}$$

where Σ_{ξ} and Π are the self-energies of ψ_{ξ} and $\phi_{<}$, respectively.

We first calculate the self-energy Π . In the momentum space, the one-loop contribution to it is of the form

$$\Pi(Q) = \sum_{\xi} \int' \frac{d^3 p}{(2\pi)^3} \int_{-\infty}^{+\infty} \frac{dp_0}{2\pi} \text{tr}[G_{\xi 0}(P) G_{\xi 0}(P+Q)] .$$

By taking the trace over the Γ matrices, Π can be written as

$$\begin{aligned} \Pi(Q) &= \frac{8}{v_{\perp}^2 v_3} \int' \frac{d^3 \tilde{p}}{(2\pi)^3} \int_{-\infty}^{+\infty} \frac{dp_0}{2\pi} \frac{p_0(p_0 + q_0) - \sum_{j=1}^3 \tilde{p}_j(\tilde{p}_j + \tilde{q}_j) - \tilde{b}^2 \sum_{j=4,5} d_j(\tilde{\mathbf{p}}_{\perp}) d_j(\tilde{\mathbf{p}}_{\perp} + \tilde{\mathbf{q}}_{\perp})}{(p_0^2 + [E(\tilde{\mathbf{p}})]^2) \{ (p_0 + q_0)^2 + [E(\tilde{\mathbf{p}} + \tilde{\mathbf{q}})]^2 \}} \\ &= \frac{4}{v_{\perp}^2 v_3} \int' \frac{d^3 \tilde{p}}{(2\pi)^3} \frac{E(\tilde{\mathbf{p}} + \tilde{\mathbf{q}})[E(\tilde{\mathbf{p}} + \tilde{\mathbf{q}}) + iq_0] + \sum_{j=1}^3 \tilde{p}_j(\tilde{p}_j + \tilde{q}_j) + \tilde{b}^2 \sum_{j=4,5} d_j(\tilde{\mathbf{p}}_{\perp}) d_j(\tilde{\mathbf{p}}_{\perp} + \tilde{\mathbf{q}}_{\perp})}{E(\tilde{\mathbf{p}} + \tilde{\mathbf{q}})[E(\tilde{\mathbf{p}} + \tilde{\mathbf{q}}) - E(\tilde{\mathbf{p}}) + iq_0][E(\tilde{\mathbf{p}} + \tilde{\mathbf{q}}) + E(\tilde{\mathbf{p}}) + iq_0]} \\ &\quad - \frac{4}{v_{\perp}^2 v_3} \int' \frac{d^3 \tilde{p}}{(2\pi)^3} \frac{E(\tilde{\mathbf{p}})[E(\tilde{\mathbf{p}}) - iq_0] + \sum_{j=1}^3 \tilde{p}_j(\tilde{p}_j + \tilde{q}_j) + \tilde{b}^2 \sum_{j=4,5} d_j(\tilde{\mathbf{p}}_{\perp}) d_j(\tilde{\mathbf{p}}_{\perp} + \tilde{\mathbf{q}}_{\perp})}{E(\tilde{\mathbf{p}})[E(\tilde{\mathbf{p}} + \tilde{\mathbf{q}}) - E(\tilde{\mathbf{p}}) + iq_0][E(\tilde{\mathbf{p}} + \tilde{\mathbf{q}}) + E(\tilde{\mathbf{p}}) - iq_0]} , \end{aligned}$$

where $E(\tilde{\mathbf{p}}) = \sqrt{\tilde{\mathbf{p}}_{\perp}^2 + \tilde{p}_3^2 + \tilde{b}^2 \tilde{\mathbf{p}}_{\perp}^4}$. From the first equality, we notice that Π is an even function of q_0 , \tilde{q}_1 , \tilde{q}_2 , and \tilde{q}_3 . Moreover, it is invariant against the exchange of variables: $\tilde{q}_1 \leftrightarrow \tilde{q}_2$. Therefore, the derivative expansion of Π is of the form

$$\Pi(Q) = \Pi(0) + \Pi_0 q_0^2 + \Pi_{\perp} \tilde{q}_{\perp}^2 + \Pi_3 \tilde{q}_3^2 + \dots ,$$

where \dots denotes the higher order terms. One may verify that $\lim_{q_0 \rightarrow 0} \lim_{\mathbf{q} \rightarrow 0} \Pi(Q) = 0 = \lim_{\mathbf{q} \rightarrow 0} \lim_{q_0 \rightarrow 0} \Pi(Q)$, and thus $\Pi(0) = 0$. This implies that the ϕ field is gapless to the one-loop order.

The expansion coefficients Π_3 and Π_{\perp} are given by

$$\begin{aligned} \Pi_3 &= \frac{1}{v_{\perp}^2 v_3} \int' \frac{d^3 \tilde{p}}{(2\pi)^3} \left\{ \frac{1}{[E(\tilde{\mathbf{p}})]^3} - \frac{\tilde{p}_3^2}{[E(\tilde{\mathbf{p}})]^5} \right\} \\ &= \frac{l}{2v_{\perp}^2 v_3 \pi^2} F_3(\delta) + O(l^2) , \end{aligned}$$

and

$$\begin{aligned} \Pi_{\perp} &= \frac{1}{v_{\perp}^2 v_3} \int' \frac{d^3 \tilde{p}}{(2\pi)^3} \left\{ \frac{1 + 4\tilde{b}^2 \mathbf{p}_{\perp}^2}{[E(\tilde{\mathbf{p}})]^3} - \frac{(1 + 2\tilde{b}^2 \mathbf{p}_{\perp}^2)^2 \mathbf{p}_{\perp}^2}{2[E(\tilde{\mathbf{p}})]^5} \right\} \\ &= \frac{l}{2v_{\perp}^2 v_3 \pi^2} F_{\perp}(\delta) + O(l^2) , \end{aligned}$$

respectively, where $\delta = \tilde{b}\Lambda$ is a dimensionless parameter and

$$\begin{aligned} F_3(z) &= \int_0^{+\infty} dt \left[\frac{1}{(t^2 + 1 + z^2)^{3/2}} - \frac{t^2}{(t^2 + 1 + z^2)^{5/2}} \right] \\ &= \frac{2}{3(1 + z^2)} , \end{aligned}$$

$$\begin{aligned} F_{\perp}(z) &= \int_0^{+\infty} dt \left[\frac{1 + 4z^2}{(t^2 + 1 + z^2)^{3/2}} - \frac{(1 + 2z^2)^2}{2(t^2 + 1 + z^2)^{5/2}} \right] \\ &= \frac{2 + 11z^2 + 8z^4}{3(1 + z^2)^2} . \end{aligned}$$

Next, we calculate the self-energy Σ_ξ of the fermionic fields. The one-loop contribution to it is of the form

$$\begin{aligned}\Sigma_\xi(Q) &= -\frac{i^2}{2} \cdot 2 \int' \frac{d^3 p}{(2\pi)^3} \int_{-\infty}^{+\infty} \frac{dp_0}{2\pi} G_{0\xi}(P) D_0(\mathbf{q} - \mathbf{p}) \\ &= \int' \frac{d^3 p}{(2\pi)^3} \int_{-\infty}^{+\infty} \frac{dp_0}{2\pi} G_{0\xi}(P) D_0(\mathbf{q} - \mathbf{p}) \\ &= \Sigma_{\xi 0}(Q) + \sum_{j=1}^5 \Sigma_{\xi j}(Q) \Gamma_j ,\end{aligned}$$

where

$$D_0(\mathbf{p}) = -\frac{g_\perp^2 g_3^2}{(g_3/v_\perp)^2 \tilde{\mathbf{p}}_\perp^2 + (g_\perp/v_3)^2 \tilde{p}_3^2} ,$$

is the free propagator of the ϕ field,

$$\begin{aligned}\Sigma_{\xi 0}(Q) &= \frac{1}{4} \text{tr}[\Sigma_\xi(Q)] \\ &= -\int' \frac{d^3 p}{(2\pi)^3} D_0(\mathbf{q} - \mathbf{p}) \int_{-\infty}^{+\infty} \frac{dp_0}{2\pi} \frac{ip_0}{p_0^2 + [E(\tilde{\mathbf{p}})]^2} \\ &= 0 ,\end{aligned}$$

and

$$\Sigma_{\xi j}(Q) = \frac{1}{4} \text{tr}[\Gamma_j \Sigma_\xi(Q)] .$$

Consequently, we find that

$$\begin{aligned}\Sigma_{\xi j}(Q) &= -\int' \frac{d^3 p}{(2\pi)^3} D_0(\mathbf{q} - \mathbf{p}) \int_{-\infty}^{+\infty} \frac{dp_0}{2\pi} \frac{\tilde{p}_j}{p_0^2 + [E(\tilde{\mathbf{p}})]^2} \\ &= -\int' \frac{d^3 p}{(2\pi)^3} \frac{\tilde{p}_j D_0(\mathbf{q} - \mathbf{p})}{2E(\tilde{\mathbf{p}})} ,\end{aligned}$$

for $j = 1, 2$,

$$\begin{aligned}\Sigma_{\xi 3}(Q) &= -\int' \frac{d^3 p}{(2\pi)^3} D_0(\mathbf{q} - \mathbf{p}) \int_{-\infty}^{+\infty} \frac{dp_0}{2\pi} \frac{\xi \tilde{p}_3}{p_0^2 + [E(\tilde{\mathbf{p}})]^2} \\ &= -\int' \frac{d^3 p}{(2\pi)^3} \frac{\xi \tilde{p}_3 D_0(\mathbf{q} - \mathbf{p})}{2E(\tilde{\mathbf{p}})} ,\end{aligned}$$

and

$$\begin{aligned}\Sigma_{\xi j}(Q) &= -\int' \frac{d^3 p}{(2\pi)^3} D_0(\mathbf{q} - \mathbf{p}) \int_{-\infty}^{+\infty} \frac{dp_0}{2\pi} \frac{\tilde{b} d_j(\mathbf{p}_\perp)}{p_0^2 + [E(\tilde{\mathbf{p}})]^2} \\ &= -\int' \frac{d^3 p}{(2\pi)^3} \frac{\tilde{b} d_j(\mathbf{p}_\perp) D_0(\mathbf{q} - \mathbf{p})}{2E(\tilde{\mathbf{p}})} ,\end{aligned}$$

for $j = 4, 5$.

To proceed, we perform the derivation expansions on $\Sigma_{\xi j}(Q)$. We notice that these functions have the following properties: (i) For $j = 1, \dots, 5$, $\Sigma_{\xi j}(0) = 0$. This can be seen as follows. For $j = 1, 2, 3$,

$$\Sigma_{\xi j}(0) \propto \int' \frac{d^3 p}{(2\pi)^3} \frac{\tilde{p}_j D_0(\mathbf{p})}{2E(\tilde{\mathbf{p}})} = 0 ,$$

because the integrand is an odd function of p_j . Next, for $j = 4$,

$$\Sigma_{\xi 4}(0) \propto \int' \frac{d^3 p}{(2\pi)^3} \frac{(\tilde{p}_2^2 - \tilde{p}_1^2) D_0(\mathbf{p})}{2E(\tilde{\mathbf{p}})} = 0 ,$$

because the integrand is odd under the exchange of variables $\tilde{p}_1 \leftrightarrow \tilde{p}_2$. Finally, for $j = 5$,

$$\Sigma_{\xi 5}(0) \propto \int' \frac{d^3 p}{(2\pi)^3} \frac{\tilde{p}_1 \tilde{p}_2 D_0(\mathbf{p})}{2E(\tilde{\mathbf{p}})} = 0 ,$$

because the integrand is an odd function of p_1 and p_2 . The fact $\Sigma_{\xi j}(0) = 0$ implies that the fermion fields are still gapless to the one-loop order. (ii) For $j = 1, 2, 3$, $\Sigma_{\xi j}(Q)$ are odd functions of q_j and even functions of $q_{i \neq j}$. (iii) $\Sigma_{\xi 4}(Q)$ is an even function of q_1, q_2 , and q_3 . Moreover, it is odd under the exchange of variables $q_1 \leftrightarrow q_2$. (iv) $\Sigma_{\xi 5}(Q)$ is an odd function of q_1 and q_2 and an even function of q_3 . Moreover, it is an even function of $\tilde{\mathbf{q}}_\perp$. Based on (i) – (iv), the derivative expansions of $\Sigma_{\xi j}(Q)$ are of the forms:

$$\Sigma_{\xi j}(Q) = \Sigma_{\xi j}^{(1)} \tilde{q}_j + \dots ,$$

for $j = 1, 2, 3$ and

$$\Sigma_{\xi j}(Q) = \Sigma_{\xi j}^{(1)} \tilde{b} d_j(\tilde{\mathbf{q}}_\perp) + \Sigma_{\xi j}^{(2)} \tilde{q}_3^2 + \dots ,$$

for $j = 4, 5$ where \dots denotes the higher order terms.

If $\Sigma_{\xi 4/5}^{(2)} \neq 0$, then we have to add additional terms to the bare action and introduce more parameters. Moreover, if $\Sigma_{\xi 4}^{(1)} \neq \Sigma_{\xi 5}^{(1)}$, we have to introduce two parameters b_1 and b_2 instead of a single one b . We will see, however, $\Sigma_{\xi 4/5}^{(2)} = 0$ and $\Sigma_{\xi 4}^{(1)} = \Sigma_{\xi 5}^{(1)}$ to the one-loop order, and thus all terms listed in the bare action form a complete set under the RG transformations, at least to the one-loop order.

These expansions coefficients can be calculated as follows.

$$\begin{aligned}\Sigma_{\xi 1/2}^{(1)} &= -\frac{g_3^2}{v_\perp^2} \int' \frac{d^3 p}{(2\pi)^3} \frac{\tilde{p}_{1/2}^2 D_0(\mathbf{p})}{E(\tilde{\mathbf{p}})[(g_3/v_\perp)^2 \tilde{\mathbf{p}}_\perp^2 + (g_\perp/v_3)^2 \tilde{p}_3^2]} \\ &= -\frac{g_3^2}{v_\perp^4 v_3} \int' \frac{d^3 \tilde{p}}{(2\pi)^3} \frac{\tilde{p}_{1/2}^2 D_0(\mathbf{p})}{E(\tilde{\mathbf{p}})[(g_3/v_\perp)^2 \tilde{\mathbf{p}}_\perp^2 + (g_\perp/v_3)^2 \tilde{p}_3^2]} \\ &= \beta^2 \alpha l G_\perp(\beta, \delta) + O(l^2) ,\end{aligned}$$

$$\begin{aligned}\Sigma_{\xi 3}^{(1)} &= -\frac{\xi g_\perp^2}{v_3^2} \int' \frac{d^3 p}{(2\pi)^3} \frac{\tilde{p}_3^2 D_0(\mathbf{p})}{E(\tilde{\mathbf{p}})[(g_3/v_\perp)^2 \tilde{\mathbf{p}}_\perp^2 + (g_\perp/v_3)^2 \tilde{p}_3^2]} \\ &= -\frac{\xi g_\perp^2}{v_\perp^2 v_3^3} \int' \frac{d^3 \tilde{p}}{(2\pi)^3} \frac{\tilde{p}_3^2 D_0(\mathbf{p})}{E(\tilde{\mathbf{p}})[(g_3/v_\perp)^2 \tilde{\mathbf{p}}_\perp^2 + (g_\perp/v_3)^2 \tilde{p}_3^2]} \\ &= \xi \beta \alpha l G_3(\beta, \delta) + O(l^2) ,\end{aligned}$$

$$\begin{aligned}
\Sigma_{\xi^4}^{(1)} &= -\frac{2g_3^4}{v_\perp^4} \int' \frac{d^3 p}{(2\pi)^3} \frac{(\tilde{p}_2^2 - \tilde{p}_1^2) \tilde{p}_2^2 D_0(\mathbf{p})}{E(\tilde{\mathbf{p}})[(g_3/v_\perp)^2 \tilde{\mathbf{p}}_\perp^2 + (g_\perp/v_3)^2 \tilde{p}_3^2]^2} \\
&= \frac{2g_\perp^2 g_3^6}{v_\perp^6 v_3} \int' \frac{d^3 \tilde{p}}{(2\pi)^3} \frac{(\tilde{p}_2^2 - \tilde{p}_1^2) \tilde{p}_2^2}{E(\tilde{\mathbf{p}})[(g_3/v_\perp)^2 \tilde{\mathbf{p}}_\perp^2 + (g_\perp/v_3)^2 \tilde{p}_3^2]^3} \\
&= \frac{g_\perp^2 g_3^6}{8v_\perp^6 v_3 \pi^2} \int_{\Lambda/s}^\Lambda d\tilde{p}_\perp \tilde{p}_\perp \int_{-\infty}^{+\infty} d\tilde{p}_3 \\
&\quad \times \frac{\tilde{p}_\perp^4}{[(g_3/v_\perp)^2 \tilde{p}_\perp^2 + (g_\perp/v_3)^2 \tilde{p}_3^2]^3 \sqrt{\tilde{p}_3^2 + \tilde{p}_\perp^2 + \tilde{b}^2 \tilde{p}_\perp^4}} \\
&= \beta^3 \alpha l G_4(\beta, \delta) + O(l^2) ,
\end{aligned}$$

$$\begin{aligned}
\Sigma_{\xi^4}^{(2)} &= -\frac{2\tilde{b}g_\perp^4}{v_\perp^4} \int' \frac{d^3 p}{(2\pi)^3} \frac{(\tilde{p}_2^2 - \tilde{p}_1^2) \tilde{p}_3^2 D_0(\mathbf{p})}{E(\tilde{\mathbf{p}})[(g_3/v_\perp)^2 \tilde{\mathbf{p}}_\perp^2 + (g_\perp/v_3)^2 \tilde{p}_3^2]^2} \\
&\quad + \frac{\tilde{b}g_\perp^4}{2v_\perp^4} \int' \frac{d^3 p}{(2\pi)^3} \frac{(\tilde{p}_2^2 - \tilde{p}_1^2) D_0(\mathbf{p})}{E(\tilde{\mathbf{p}})[(g_3/v_\perp)^2 \tilde{\mathbf{p}}_\perp^2 + (g_\perp/v_3)^2 \tilde{p}_3^2]} \\
&= 0 ,
\end{aligned}$$

and

$$\begin{aligned}
\Sigma_{\xi^5}^{(1)} &= -\frac{2g_3^4}{v_\perp^4} \int' \frac{d^3 p}{(2\pi)^3} \frac{2\tilde{p}_1^2 \tilde{p}_2^2 D_0(\mathbf{p})}{E(\tilde{\mathbf{p}})[(g_3/v_\perp)^2 \tilde{\mathbf{p}}_\perp^2 + (g_\perp/v_3)^2 \tilde{p}_3^2]^2} \\
&= \frac{2g_\perp^2 g_3^6}{v_\perp^6 v_3} \int' \frac{d^3 \tilde{p}}{(2\pi)^3} \frac{2\tilde{p}_1^2 \tilde{p}_2^2}{E(\tilde{\mathbf{p}})[(g_3/v_\perp)^2 \tilde{\mathbf{p}}_\perp^2 + (g_\perp/v_3)^2 \tilde{p}_3^2]^3} \\
&= \frac{g_\perp^2 g_3^6}{8v_\perp^6 v_3 \pi^2} \int_{\Lambda/s}^\Lambda d\tilde{p}_\perp \tilde{p}_\perp \int_{-\infty}^{+\infty} d\tilde{p}_3 \\
&\quad \times \frac{\tilde{p}_\perp^4}{[(g_3/v_\perp)^2 \tilde{p}_\perp^2 + (g_\perp/v_3)^2 \tilde{p}_3^2]^3 \sqrt{\tilde{p}_3^2 + \tilde{p}_\perp^2 + \tilde{b}^2 \tilde{p}_\perp^4}} \\
&= \Sigma_{\xi^4}^{(1)} ,
\end{aligned}$$

$$\begin{aligned}
\Sigma_{\xi^5}^{(2)} &= -\frac{2\tilde{b}g_\perp^4}{v_\perp^4} \int' \frac{d^3 p}{(2\pi)^3} \frac{2\tilde{p}_1 \tilde{p}_2 \tilde{p}_3^2 D_0(\mathbf{p})}{E(\tilde{\mathbf{p}})[(g_3/v_\perp)^2 \tilde{\mathbf{p}}_\perp^2 + (g_\perp/v_3)^2 \tilde{p}_3^2]^2} \\
&\quad + \frac{\tilde{b}g_\perp^4}{2v_\perp^4} \int' \frac{d^3 p}{(2\pi)^3} \frac{2\tilde{p}_1 \tilde{p}_2 D_0(\mathbf{p})}{E(\tilde{\mathbf{p}})[(g_3/v_\perp)^2 \tilde{\mathbf{p}}_\perp^2 + (g_\perp/v_3)^2 \tilde{p}_3^2]} \\
&= 0 ,
\end{aligned}$$

where $\beta = \eta/r^2$ and

$$\begin{aligned}
G_\perp(\beta, z) &= \int_0^{+\infty} \frac{dt}{(t^2 + \beta)^2 \sqrt{t^2 + 1 + z^2}} , \\
G_3(\beta, z) &= \int_0^{+\infty} dt \frac{2t^2}{(t^2 + \beta)^2 \sqrt{t^2 + 1 + z^2}} , \\
G_4(\beta, z) &= \int_0^{+\infty} \frac{dt}{(t^2 + \beta)^3 \sqrt{t^2 + 1 + z^2}} .
\end{aligned}$$

Finally, we calculate the one-loop contribution to the vertex function, which arises from I_3 :

$$\begin{aligned}
I_3 &= \frac{1}{6} \langle S_{int}^3 \rangle + I_1 I_2 - \frac{1}{6} I_1^3 = \frac{1}{6} \langle S_{int}^3 \rangle \\
&= i\Gamma_v \int_X \phi_{<} \rho_{0<} + \dots ,
\end{aligned}$$

where \dots denotes the terms with higher scaling dimensions. In view of S_{int} , Γ_v is given by

$$\begin{aligned}
\Gamma_v &= (-i) \frac{i^3}{6} \cdot 3 \cdot 2 \sum_\xi \int' \frac{d^3 p}{(2\pi)^3} \int_{-\infty}^{+\infty} \frac{dp_0}{2\pi} [-D_0(-\mathbf{p})] \\
&\quad \times [G_{0\xi}(P)]^2 \\
&= -\sum_\xi \int' \frac{d^3 p}{(2\pi)^3} D_0(-\mathbf{p}) \int_{-\infty}^{+\infty} \frac{dp_0}{2\pi} \frac{p_0^2 - [E(\tilde{\mathbf{p}})]^2}{(p_0^2 + [E(\tilde{\mathbf{p}})]^2)^2} \\
&= 0 .
\end{aligned}$$

As we have shown that $\Sigma_\tau = 0$ to the one-loop order, this result indicates that our one-loop calculation is consistent with the Ward identity [Eq. (B2)], and thus respects the gauge invariance.

Collecting the above results, S_{eff} to the one-loop order is of the form

$$\begin{aligned}
S_{eff}[\psi_{<}, \psi_{<}^\dagger, \phi_{<}] &= \sum_\xi \int_X \psi_{\xi<}^\dagger \partial_\tau \psi_{\xi<} + [1 + \beta^2 \alpha l G_\perp(\beta, \delta) + O(l^2)] \sum_\xi \sum_{j=1,2} \int_X \psi_{\xi<}^\dagger \Gamma_j v_\perp (-i\partial_j \psi_{\xi<}) \\
&\quad + [1 + \beta \alpha l G_3(\beta, \delta) + O(l^2)] \sum_\xi \int_X \psi_{\xi<}^\dagger \Gamma_3 \xi v_3 (-i\partial_3 \psi_{\xi<}) \\
&\quad + [1 + \beta^3 \alpha l G_4(\beta, \delta) + O(l^2)] \sum_\xi \sum_{j=4,5} \int_X \psi_{\xi<}^\dagger \Gamma_j b d_j (-i\nabla) \psi_{\xi<} + i \int_X \phi_{<} \rho_{0<} \\
&\quad + \frac{1}{2} \int_X \left\{ \left[\frac{1}{g_\perp^2} + \frac{l}{2v_3 \pi^2} F_\perp(\delta) + O(l^2) \right] |\nabla_\perp \phi_{<}|^2 + \left[\frac{1}{g_3^2} + \frac{l}{2rv_\perp \pi^2} F_3(\delta) + O(l^2) \right] |\partial_3 \phi_{<}|^2 \right\} + \dots ,
\end{aligned}$$

where \dots denotes the terms with higher scaling dimensions. Now we perform the scaling transformation

$$x(y) \rightarrow e^l x(y), \quad z \rightarrow e^{z_3 l} z, \quad \tau \rightarrow e^{z l} \tau, \quad \psi_{\xi <} = Z_{\psi}^{-1/2} \psi_{\xi}, \quad \phi_{<} = Z_{\phi}^{-1/2} \phi,$$

to bring the terms $\int_X \psi_{\xi}^{\dagger} \partial_{\tau} \psi_{\xi <}$ and $i \int_X \phi_{<} \rho_{0 <}$ back to their original forms, yielding $Z_{\psi} = e^{(2+z_3)l}$ and $Z_{\phi} = e^{2zl}$. Therefore, S_{eff} becomes

$$\begin{aligned} S_{eff}[\psi, \psi^{\dagger}, \phi] &= \sum_{\xi} \int_X \psi_{\xi}^{\dagger} \partial_{\tau} \psi_{\xi} + e^{(z-1)l} [1 + \beta^2 \alpha l G_{\perp}(\beta, \delta) + O(l^2)] \sum_{\xi} \sum_{j=1,2} \int_X \psi_{\xi}^{\dagger} \Gamma_j v_{\perp} (-i \partial_j \psi_{\xi}) \\ &\quad + e^{(z-z_3)l} [1 + \beta \alpha l G_3(\beta, \delta) + O(l^2)] \sum_{\xi} \int_X \psi_{\xi}^{\dagger} \Gamma_3 \xi v_3 (-i \partial_3 \psi_{\xi}) \\ &\quad + e^{(z-2)l} [1 + \beta^3 \alpha l G_4(\beta, \delta) + O(l^2)] \sum_{\xi} \sum_{j=4,5} \int_X \psi_{\xi}^{\dagger} \Gamma_j b d_j (-i \nabla) \psi_{\xi} \\ &\quad + \frac{1}{2} e^{(z_3-z)l} \left[\frac{1}{g_{\perp}^2} + \frac{l}{2v_3 \pi^2} F_{\perp}(\delta) + O(l^2) \right] \int_X |\nabla_{\perp} \phi|^2 \\ &\quad + \frac{1}{2} e^{(2-z-z_3)l} \left[\frac{1}{g_3^2} + \frac{l}{2rv_{\perp} \pi^2} F_3(\delta) + O(l^2) \right] \int_X |\partial_3 \phi|^2 + i \int_X \phi \rho_0 + \dots \end{aligned}$$

Consequently, the one-loop recursion relations for the parameters v_{\perp} , v_3 , b , g_{\perp}^2 , and g_3^2 are

$$\begin{aligned} \frac{v'_{\perp}}{v_{\perp}} &= e^{(z-1)l} [1 + \beta^2 \alpha l G_{\perp}(\beta, \delta) + O(l^2)] = 1 + (z-1)l + \beta^2 \alpha l G_{\perp}(\beta, \delta) + O(l^2), \\ \frac{v'_3}{v_3} &= e^{(z-z_3)l} [1 + \beta \alpha l G_3(\beta, \delta) + O(l^2)] = 1 + (z-z_3)l + \beta \alpha l G_3(\beta, \delta) + O(l^2), \\ \frac{b'}{b} &= e^{(z-2)l} [1 + \beta^3 \alpha l G_4(\beta, \delta) + O(l^2)] = 1 + (z-2)l + \beta^3 \alpha l G_4(\beta, \delta) + O(l^2), \\ \frac{g_{\perp}^2}{(g'_{\perp})^2} &= e^{(z_3-z)l} [1 + 2\alpha l F_{\perp}(\delta) + O(l^2)] = 1 - (z-z_3)l + 2\alpha l F_{\perp}(\delta) + O(l^2), \\ \frac{g_3^2}{(g'_3)^2} &= e^{(2-z-z_3)l} [1 + 2\beta \alpha l F_3(\delta) + O(l^2)] = 1 - (z+z_3-2)l + 2\beta \alpha l F_3(\delta) + O(l^2). \end{aligned}$$

We choose the values of z and z_3 such that v_3 and b are both RG invariants, which leads to Eq. (19). Therefore, the one-loop recursion relations for the other parameters become

$$\begin{aligned} \frac{r'}{r} &= 1 + [1 + \beta^2 \alpha G_{\perp}(\beta, \delta) - \beta^3 \alpha G_4(\beta, \delta)]l + O(l^2), \\ \frac{\delta'}{\delta} &= 1 - [3 + 2\beta^2 \alpha G_{\perp}(\beta, \delta) - 2\beta^3 \alpha G_4(\beta, \delta)]l + O(l^2), \\ \frac{g_{\perp}^2}{(g'_{\perp})^2} &= 1 + [\beta \alpha G_3(\beta, \delta) + 2\alpha F_{\perp}(\delta)]l + O(l^2), \\ \frac{g_3^2}{(g'_3)^2} &= 1 - [2 + \beta \alpha G_3(\beta, \delta) - 2\beta^3 \alpha G_4(\beta, \delta) - 2\beta \alpha F_3(\delta)]l + O(l^2). \end{aligned}$$

Note that $\delta' = b' \Lambda' / (v'_{\perp})^2 = [b' / (v'_{\perp})^2] \Lambda e^{-l}$. From these one-loop recursion relations, we obtain Eqs. (20) – (23).

* Electronic address: ywlee@thu.edu.tw

† Electronic address: ylee@cc.ncue.edu.tw

¹ M.Z. Hasan and C.L. Kane, Rev. Mod. Phys. **82**, 3045 (2010).

² X.-L. Qi and S.-C. Zhang, Rev. Mod. Phys. **83**, 1057 (2011).

³ C.-K. Chiu, J.C.Y. Teo, A.P. Schnyder, and S. Ryu, Rev. Mod. Phys. **88**, 035005 (2016).

- ⁴ P. Hosur and X.-L. Qi, C.R. Physique **14**, 857 (2013).
- ⁵ N.P. Armitage, E.J. Mele, and A. Vishwanath, Rev. Mod. Phys. **90**, 015001 (2018).
- ⁶ B.J. Yang, E.G. Moon, H. Isobe, and N. Nagaosa, Nat. Phys. **10**, 774 (2014).
- ⁷ G. Xu, H. Weng, Z. Wang, X. Dai, and Z. Fang, Phys. Rev. Lett. **107**, 186806 (2011).
- ⁸ C. Fang, M.J. Gilbert, X. Dai, and B.A. Bernevig, Phys. Rev. Lett. **108**, 266802 (2012).
- ⁹ A.A. Soluyanov, D. Gresch, Z. Wang, Q. Wu, M. Troyer, X. Dai, and B.A. Bernevig, Nature **527**, 495 (2015).
- ¹⁰ W.A. Benalcazar, B.A. Bernevig, and T.L. Hughes, Science **357**, 61 (2017).
- ¹¹ S.A. Parameswaran and Y. Wan, Physics **10**, 132 (2017).
- ¹² W.A. Benalcazar, B.A. Bernevig, and T.L. Hughes, Phys. Rev. **B96**, 245115 (2017).
- ¹³ M. Lin and T.L. Hughes, Phys. Rev. **B98**, 241103(R) (2018).
- ¹⁴ D. Čalugăru, V. Juričić, and B. Roy, Phys. Rev. **B99**, 041301(R) (2019).
- ¹⁵ A.L. Szabó and B. Roy, Phys. Rev. Research **2**, 043197 (2020).
- ¹⁶ H.-X. Wang, Z.-K. Lin, B. Jiang, G.-Y. Guo, and J.-H. Jiang, Phys. Rev. Lett. **125**, 146401 (2020).
- ¹⁷ S.A.A. Ghorashi, T. Li, and T.L. Hughes, Phys. Rev. Lett. **125**, 266804 (2020).
- ¹⁸ S.M. Young, S. Zaheer, J.C.Y. Teo, C.L. Kane, E.J. Mele, and A.M. Rappe, Phys. Rev. Lett. **108**, 140405 (2012).
- ¹⁹ M. Kargarian, M. Randeria, and Y.-M. Lu, Proc. Natl. Acad. Sci. **113**, 8648 (2016).
- ²⁰ B.J. Wieder, Z. Wang, J. Cano, X. Dai, L.M. Schoop, B. Bradlyn, and B.A. Bernevig, Nat. Commun. **11**, 627 (2020).
- ²¹ C.-Z. Li, A.-Q. Wang, C. Li, W.-Z. Zheng, A. Brinkman, D.-P. Yu, and Z.-M. Liao, Phys. Rev. Lett. **124**, 156601 (2020).
- ²² P. Goswami and S. Chakravarty, Phys. Rev. Lett. **107**, 196803 (2011).
- ²³ P. Hosur, S.A. Parameswaran, and A. Vishwanath, Phys. Rev. Lett. **108**, 046602 (2012).
- ²⁴ R.E. Throckmorton, J. Hofman, E. Barnes, and S. Das Sarma, Phys. Rev. **B92**, 115101 (2015).
- ²⁵ Without breaking the P and T symmetries, we can add a constant to g_3 : $g_3(\mathbf{k}) = -t_3(C_3 - \gamma + 2 - C_1 - C_2)$, where γ is real. For $|\gamma| < 1$, there are still two Dirac points located at $(0, 0, \pm k_0)$ where $k_0 = \cos^{-1} \gamma$.
- ²⁶ The first BZ of this model consists of 2D band structures parametrized by k_z . When $b = 0$, the T symmetry is preserved, and these 2D band structures are divided into two phases: trivial insulators and the quantum spin Hall insulators (QSHIs), separated by the two planes with $k_z = \pm k_0$. For a sample with open boundaries in the x or y directions, there are double Fermi arcs terminated at the projections of the two Dirac nodes on the surface BZ. This is the first-order DSM. When $b \neq 0$, the T symmetry is broken, and thus the edge modes are gapped. The region occupied by trivial insulators remains intact, while the QSHIs become second-order TIs. For a cube-shaped material, there will be gapless hinge modes at the hinges parallel to the z -axis and terminated at the projections of the two Dirac nodes on the surface BZ. This is the second-order DSM.
- ²⁷ H.-H. Lai, Phys. Rev. **B91**, 235131 (2015).
- ²⁸ S.-K. Jian and H. Yao, Phys. Rev. **B92**, 045121 (2015).
- ²⁹ A. Sekine and K. Nomura, Phys. Rev. **B90**, 075137 (2014).
- ³⁰ J. González, Phys. Rev. **B90**, 121107(R) (2014); Phys. Rev. **B92**, 125115 (2015).
- ³¹ D.E. Sheehy and J. Schmalian, Phys. Rev. Lett. **99**, 226803 (2007).
- ³² I.S. Gradshteyn and I.M. Ryzhik, *Tables of Integrals, Series, and Products*, 7th ed., (Academic press, California, USA, 2007).